Monosized dripping mode of axisymmetric flow focusing

Francisco Cruz-Mazo,[1,2] J. M. Montanero,[1] and A. M. Gañán-Calvo[2]
[1]*Departamento de Ingeniería Mecánica, Energética y de los Materiales and Instituto de Computación Científica Avanzada, Universidad de Extremadura, E-06006 Badajoz, Spain*
[2]*Departamento de Ingeniería Aeroespacial y Mecánica de Fluidos, Universidad de Sevilla, E-41902 Sevilla, Spain*
(Received 9 April 2016; revised manuscript received 14 June 2016; published 29 November 2016)

We identify and analyze the perfectly regular dripping mode of flow focusing. This mode occurs within narrow intervals of injected flow rates and applied pressure drops and leads to homogeneous-size droplets with diameters similar to or smaller than that of the discharge orifice. The balance between the local acceleration of the fluid particle and the applied pressure drop yields the scaling law for the droplet diameter. This scaling law is validated experimentally with excellent accord.

DOI: 10.1103/PhysRevE.94.053122

I. INTRODUCTION

The controlled fragmentation of a continuous phase is an essential prerequisite for a multitude of technological applications in varied fields, such as pharmacy, biotechnology, and the food and agriculture industry. This fragmentation can be produced by adequately manipulating matter in its fluid form and subsequently solidifying it (if necessary). In the droplet-based microfluidics context, the production of micrometer fluid entities such as drops, bubbles, emulsions, and capsules has been extensively investigated over the past 30 years. Attention has been paid to two properties owing to their great technological relevance: the size of the fluidic individuals and the monodispersity degree of the population. Experience has repeatedly shown that these features are somehow antagonistic, i.e., the smaller sizes are reached only at the expense of monodispersity and vice versa.

In order to overcome the resistance offered by both surface tension and viscosity on the micrometer or nanometer scale, use has been made of a wide range of energy sources including surfactants, electrical forces, thermal gradients, and coflows. Extensional flows constitute a remarkable class of techniques in which an externally induced pressure gradient stretches an interface until a small drop or jet is emitted [1]. In particular, axisymmetric flow focusing [2] has become very popular, especially in pharmacy [3] and biotechnology [4], because it leads to a high-rate production of monodisperse droplets, bubbles, and capsules with diameters ranging from the submillimeter to the micrometer scale [5–7].

If the dispersed phase is a liquid, the axisymmetric flow focusing works in the so-called jetting regime (Fig. 1, left). In this case, capillary jets much thinner than the discharge orifice are steadily produced in the laminar regime by applying sufficiently high pressure drops to the external gas stream [2,8–10]. These jets are characterized by Weber numbers (the ratio of the jet's speed to the capillary velocity) much higher than unity [11], which guarantees that the capillary waves spontaneously growing over the jet's free surface are swept away by the liquid stream [12,13]. These waves make the liquid ligament break up downstream into a relatively monodisperse stream of droplets whose size is commensurate with that of the precursor ligament. The droplet size homogeneity decreases due to (i) the absence of any filter for the wave number of the capillary wave leading to the jet's breakup, (ii) the formation of satellite droplets due to nonlinearities in the breakup process, and (iii) whipping instabilities triggered by the high-speed gas stream.

The jetting regime is much more difficult to reach when the dispersed phase is a gas (especially for high surface tensions), because the low density of the gaseous jet prevents overcoming the Weber-number-equals-unity barrier. In this case, the axisymmetric flow focusing operates in the so-called bubbling (or gaseous-dripping) mode, where bubbles with diameters similar to or smaller than that of the discharge orifice periodically form right behind that orifice (at distances from the discharge orifice smaller than the orifice diameter) [14]. In general, bubbles generated in this mode are exceedingly more monodisperse than the droplets produced in the jetting regime. The fact that the free surface pinch-off occurs at distances from the feeding capillary on the order of its diameter allows capillarity to act as a wave filter, which results in very narrow size distributions of the detached bubbles.

A phenomenon similar to the formation of microbubbles in a coflowing liquid has been widely studied in liquid-liquid planar flow focusing since its inception [15], with thousands of references in the literature and a wide spectrum of technological applications [16,17]. Emulsions consisting of monodisperse collections of droplets are produced with these microfluidic devices. The size of those droplets is commensurate with that of the microfluidic channel. Much less attention has been devoted to the gaseous focusing of a low- to moderate-viscosity liquid stream leading to dripping. A natural question is whether the perfectly regular dripping counterpart of bubbling [14] can be identified in that case. We show here that the answer is affirmative, its physics is similar to the bubbling case, and the outcome is considerably different from that of the relatively well studied case of the dripping faucet [18] (above all is the fact that the droplets are significantly smaller in the phenomenon analyzed here).

In the monosized dripping mode studied in this work, drops are ejected right behind the discharge orifice with diameters that are commensurate with that of the orifice. The existence of a filter (the feeding capillary-discharge orifice arrangement) for the breakup wave number and the absence of both satellite droplets and whipping instabilities enable the production of perfectly monodisperse collections of droplets. Their diameters, which are much smaller than those

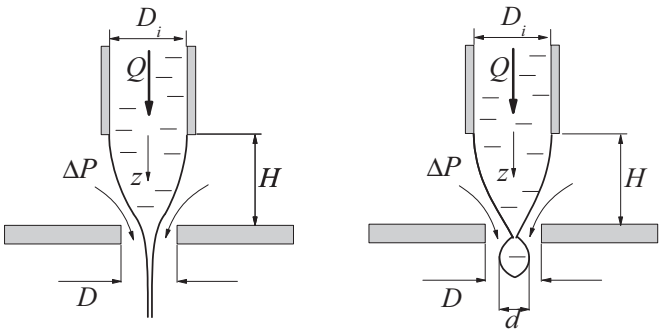

FIG. 1. Sketch of the axisymmetric flow focusing configuration: steady jetting regime (left) and monosized dripping mode (right).

obtained when a liquid simply drips from a faucet, are ideal for a range of technological applications. In addition, the Weber number takes much lower values than in the jetting regime, which reduces significantly the splashing on solid surfaces and favors the coalescence of the produced droplets with others. Finally, the coflowing gaseous stream moves slower than in the jetting regime, reducing possible undesired effects in potential applications. These features considerably widen the range of applicability of the flow focusing technique.

The purpose of the present work is to analyze the production of liquid droplets with axisymmetric flow focusing working in the monosized dripping mode. We will show that there are relatively narrow intervals of injected flow rates and applied pressure drops for the monosized dripping mode to arise. Owing to the pulsatile character of this regime, the pressure drop applied to the gas stream is essentially balanced by the fluid particle local acceleration, which constitutes the fundamental difference with respect to the steady jetting mode. Based on this idea, we will derive the scaling law for the droplet diameter as a function of the governing parameters. This scaling law will be validated experimentally.

The monosized dripping mode of flow focusing is properly identified in this work, although the transition from jetting to regular dripping has been observed in some previous experiments [19,20]. In fact, it is well known that if the coflowing gas speed falls below a certain threshold, the capillary velocity becomes on the order of the jet's speed and growing capillary waves move upstream and pinch the free surface at the discharge orifice (the convective-to-absolute instability transition [21]). In this case, the jetting regime becomes unstable and yields a dripping mode with a variety of outcomes comparable to that observed in the so-called dripping faucet problem [18,22]. Under certain conditions, the convective-to-absolute instability transition leads to the emission of monodisperse collections of droplets from a perfectly steady liquid meniscus [19,20]. This specific regime can be regarded as a particular case of the monosized dripping mode studied here. As will be shown, the parameter conditions leading to the monosized dripping mode do not necessarily coincide with those of the convective-to-absolute instability transition. In addition, the liquid meniscus tip may either remain steady or oscillate depending on both the liquid viscosity and the meniscus aspect ratio. On the other hand, the narrow parameter windows leading to the monosized dripping mode contrast with the much wider conditions for regular dripping in (planar or axisymmetric) liquid-liquid flow focusing [15,23].

II. MONOSIZED DRIPPING VERSUS STEADY JETTING

Consider the axisymmetric flow focusing sketched in Fig. 1. A liquid current of density ρ and viscosity μ is injected at a constant flow rate Q through a feeding capillary of inner diameter D_i, located at a distance H from a discharge orifice of diameter D. A gaseous stream, driven by an applied pressure drop ΔP, stretches and focuses the liquid meniscus hanging on the edge of the feeding capillary so that both the liquid and air currents cross the discharge orifice. In the steady jetting regime (Fig. 1, left), the meniscus tapers to a thin jet, which breaks up downstream due to the growth of capillary waves. In contrast, a droplet of diameter d forms right behind the discharge orifice in the monosized dripping mode (Fig. 1, right).

III. SCALING ANALYSIS

The projection of the momentum equation onto the symmetry z axis (Fig. 1) and evaluated at that axis reads

$$\frac{\partial u}{\partial t}+u\frac{\partial u}{\partial z}=-\frac{1}{\rho}\frac{\partial p}{\partial z}+\frac{\mu}{\rho}\frac{\partial^2 u}{\partial z^2}, \tag{1}$$

where u and p are the z components of the velocity and pressure in the liquid domain, respectively, only the dominant contribution to the viscosity term has been retained, and the gravitational force has been neglected due to the smallness of the fluid configuration. In the monosized dripping mode, the orders of magnitude of the terms in Eq. (1) are

$$\begin{aligned}&\frac{\partial}{\partial t}\sim\frac{Q}{d^3},\quad u\sim\frac{Q}{d^2},\quad u\frac{\partial u}{\partial z}\sim\frac{Q^2}{d^4D_i},\\&\frac{\partial p}{\partial z}\sim\frac{\Delta P_l}{D_i},\quad \frac{\mu}{\rho}\frac{\partial^2 u}{\partial z^2}\sim\frac{\mu}{\rho}\frac{Q}{d^2D_i^2},\end{aligned} \tag{2}$$

where ΔP_l is the pressure drop across the liquid meniscus and we have taken into account that $D_i\sim H$. In fact, for $H\ll D_i, D$ flow focusing gives rise to Flow Blurring® [24], while for $H\gg D_i, D$ the liquid meniscus becomes fully unstable and the liquid ejection interrupts (a drop much larger than the discharge orifice forms at that orifice) [20].

In the steady jetting regime, the pressure drop $\partial p/\partial z$ induced by the outer gaseous stream essentially transforms into the convective term $u\partial u/\partial z$ (the jet's kinetic energy). In contrast, the convective term becomes at most comparable to the unsteady contribution to the fluid particle acceleration in the monosized dripping mode, owing to the pulsatile character of the latter. This constitutes the fundamental difference between these two operational regimes of flow focusing and justifies why the drop inflation time d^3/Q is selected as the characteristic time of the process. In addition, the Womersley number $\alpha=QD_i^2\rho/\mu d^3$ (which measures the relative importance of local acceleration versus viscosity force) takes large values for small and moderate liquid viscosities and therefore viscous stresses can be neglected too. Considering

the dominant terms in Eq. (1), one gets

$$\frac{Q^2}{d^5} \sim \frac{\Delta P_l}{\rho D_i}. \tag{3}$$

On the other hand, the fact that the convective term is at most comparable to the unsteady term implies that $d \lesssim D_i$ and

$$\frac{Q^2}{d^4 D_i} \lesssim \frac{\Delta P_l}{\rho D_i}. \tag{4}$$

If one assumes, as a first approximation, that the free surface breakup time t_b is not essentially affected by the external parameters D_i, Q, and ΔP, then dimensional analysis dictates that $t_b \sim t_c^* = (\rho d^3/\sigma)^{1/2}$ (t_c^* is the capillary time defined in terms of the droplet diameter and σ is the surface tension) for sufficiently low viscosities. The droplet forms during a time of the order of t_b and therefore $t_b \sim d^3/Q$. This condition reduces to $Q \sim \sigma^{1/2}\rho^{-1/2}d^{3/2}$, which allows one to eliminate the flow rate Q from Eq. (3). In addition, that condition together with (4) implies that $\sigma/d \lesssim \Delta P_l$ and therefore the pressure drop across the liquid meniscus is of the order of that applied in the outer gaseous stream, i.e., $\Delta P_l \sim \Delta P$. Thus, surface tension triggers the instability, which ultimately pinches the free surface and stops the droplet formation, but it does not provide the energy necessary for that process.

Taking into account the above considerations, Eq. (3) yields the scaling law

$$\frac{d}{D_i} \sim \left(\frac{\sigma}{D_i \Delta P}\right)^{1/2} \tag{5}$$

for the droplet diameter. The secondary effect of the flow rate on the droplet diameter resembles what occurs in gravitational dripping from a faucet for relatively small values of Q, where the droplet diameter is essentially determined by the liquid density and surface tension, as well as by the orifice diameter and gravity. In this analogy, the gravitational force is somehow replaced by the applied pressure gradient $\Delta P/\rho D_i$ of monosized dripping.

IV. EXPERIMENT

We conducted experiments to validate the scaling law (5). We made use of two flow focusing devices with $D = 100$ μm and $H = 200$ μm and with $D = 200$ μm and $H = 100$ μm (Fig. 2), respectively. The feeding capillary inner diameter was $D_i = 150$ μm in both cases. The liquid was injected with a syringe pump (Harvard Apparatus PHD 4400), while the air stream was supplied by a pneumatic circuit connected to a pressure regulator and a manometer. Both the air stream and the liquid droplets are discharged to the atmosphere. The images were acquired with a high-speed camera (Hyper Vision HPV-2 Shimadzu) and processed with the open software IMAGEJ to measure the droplet diameter. We collected more than 200 experimental data using the liquids indicated in Table I. As can be observed, the viscosity ranged from low to moderately high values. Figure 3 shows the parameter windows where monosized dripping was found for the least and most viscous liquids. The upper boundaries indicate the transition between steady jetting and monosized dripping, while the lower ones correspond to the minimum values of ΔP below which the liquid ejection interrupt.

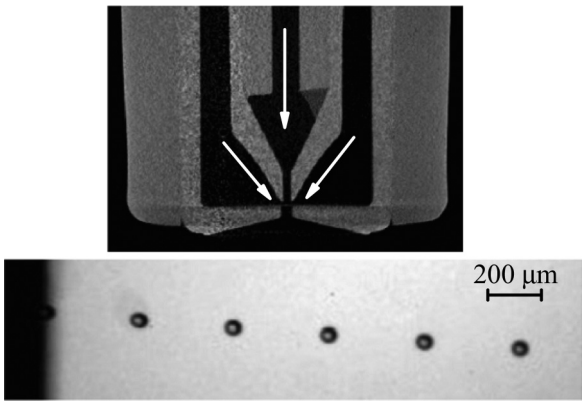

FIG. 2. The top image is a rendering of an x-ray microtomogram of the flow focusing device with $D = 200$ μm and $H = 100$ μm. The bottom image is the monosized dripping produced with water, $Q = 25$ ml/h, and $\Delta P = 41$ mbars.

Figure 4 shows the values of the ratio $t_c^*/(d^3/Q)$ and the Womersley number α in all the experimental realizations. The approximations $t_c^* \sim d^3/Q$ and $\alpha \gg 1$ are consistent with most of the experimental data. It must be noted that the droplet formation starts before the free surface pinch-off begins. Therefore, the breakup time may be significantly smaller than the droplet formation time d^3/Q, which explains why $t_c^* \lesssim d^3/Q$ in Fig. 4.

The diameters of the drops produced in the monosized dripping mode are shown in Fig. 5. The best fit to those diameters is the function

$$\frac{d}{D_i} = 1.7\left(\frac{\sigma}{D_i \Delta P}\right)^{1/2}, \tag{6}$$

with a normalized Pearson regression coefficient $R^2 = 0.913$. As anticipated from the scaling analysis, $d \lesssim D_i$. The scattering of the experimental data around (6) can be attributed to viscosity effects. The standard deviation of the droplet size histogram was smaller than the experimental uncertainty (around 3%) in all the cases analyzed. We have verified that satellite droplets appear for viscosities higher than those considered in our study.

The scaling law (6) may disguise an important aspect of the phenomenon here described: both the pressure drop ΔP and the liquid flow rate Q are control parameters of the system. Although Eq. (6) contains the applied pressure drop only, those two parameters can be independently adjusted within

TABLE I. Physical properties of the liquids used in the experiments. In the last column, the first and second symbols stand for $H/D = 0.5$ and 2, respectively, in Figs. 3–7.

Liquid	ρ (kg/m^3)	μ (mPa·s)	σ (mN/m)	Symbols
water	997	1	72	⬡/★
water + glycerol 50/50 vol %	1030	6.2	66	◀/▶
water + glycerol 40/60 vol %	1156	12.3	65	▼/◆
water + glycerol 30/70 vol %	1182	24.3	64	●/▲
ethanol	790	1.2	23	/■

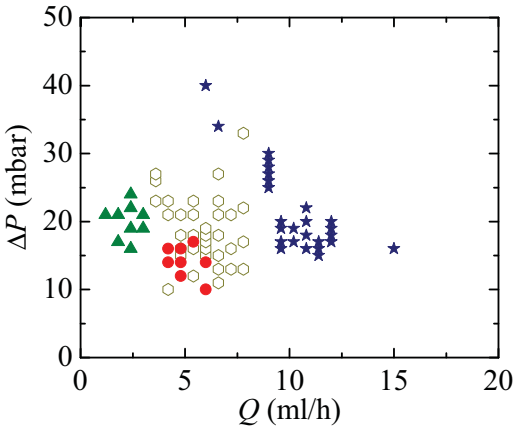

FIG. 3. Parameter windows where monosized dripping was found for water and water plus glycerol 30/70 vol %.

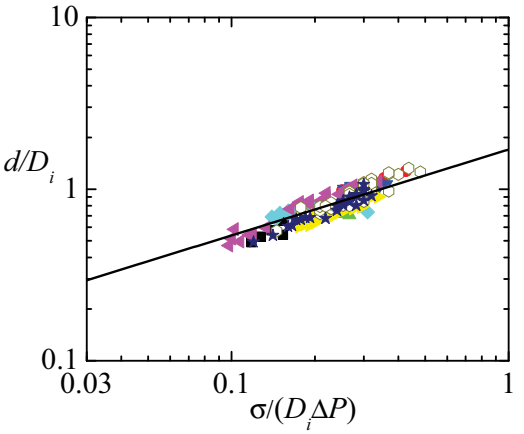

FIG. 5. Diameters of the drops produced in the monosized dripping mode. The solid line is the function $d/D_i = 1.7(\sigma/D_i\Delta P)^{1/2}$.

the parameter range shown in Fig. 3. In fact, the droplet generation frequency f can be continuously varied, without changing the droplet size, by varying the liquid flow rate while keeping the applied pressure drop constant. This implies that the droplet generation frequency does not necessarily belong to the discrete set of eigenfrequencies of the liquid meniscus. To demonstrate this, we represent in Fig. 6 the droplet generation frequency f as a function of the flow rate Q. The frequency was made dimensionless with the capillary time $t_c = (\rho D_i^3/\sigma)^{1/2}$ defined in terms of the feeding capillary diameter, while the flow rate was expressed in terms of the characteristic quantity $Q_\sigma = (\sigma^4/\rho\Delta P^3)^{1/2}$. There is a continuous distribution of the experimental measurements along the two axes, with no trace of discontinuities associated with the discrete set of meniscus eigenfrequencies [25,26]. The data are fitted by a power law with exponent unity within the experimental uncertainty and therefore Eq. (6) is recovered.

A natural question is whether the monosized dripping mode analyzed here corresponds to the onset of the absolute instability of the flow focusing steady jetting regime and therefore the parameter conditions leading to this mode are those predicted by the spatiotemporal stability analysis of that configuration [27]. Figure 7 shows all the experimental realizations projected onto the plane defined by the Reynolds and Weber numbers

$$\mathrm{Re} = \frac{\rho V_{SJ} R_{SJ}}{\mu}, \quad \mathrm{We} = \frac{\rho V_{SJ}^2 R_{SJ}}{\sigma}, \tag{7}$$

where $V_{SJ} = Q/\pi R_{SJ}^2$ and $R_{SJ} = (\rho Q^2/2\pi^2\Delta P)^{1/4}$ are the jet's velocity and radius calculated assuming the steady jetting regime, respectively [2]. The figure also shows the curve corresponding to the convective-to-absolute instability transition calculated by Leib and Goldstein [27]. As can be observed, monosized dripping was found for parameter conditions significantly far away from that instability transition. In the more viscous cases, the Weber numbers were larger than those for which absolute instability arises in the jet, while the opposite occurs for the least viscous liquid. Therefore, monosized dripping is not necessarily linked to the appearance of absolute instability in the emitted jet. The fact that the monosized dripping mode is found for Weber numbers larger than those of the convective-to-absolute instability transition suggests that, in this case, this mode originates from an instability in the tapering meniscus (not in the emitted jet) [20].

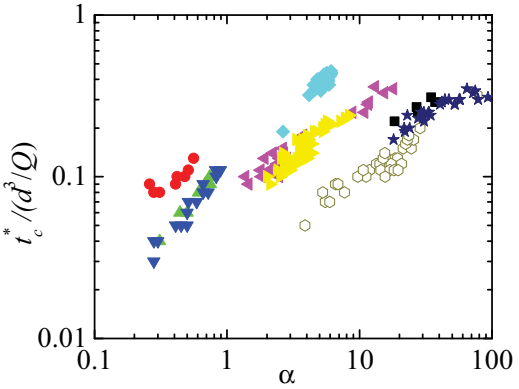

FIG. 4. Ratio $t_c^*/(d^3/Q)$ and the Womersley number α in all the experimental realizations.

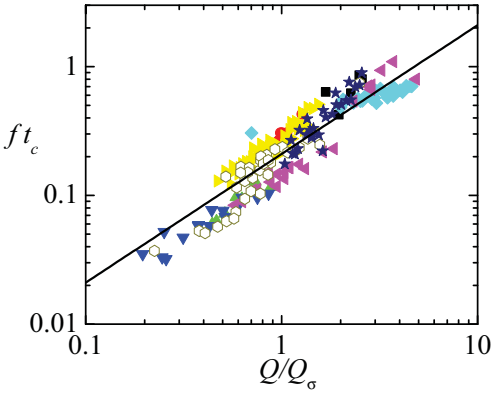

FIG. 6. Droplet production frequency f as a function of the liquid flow rate Q. The line is the fit $ft_c = 0.21(Q/Q_\sigma)^{1.04}$ to the experimental data.

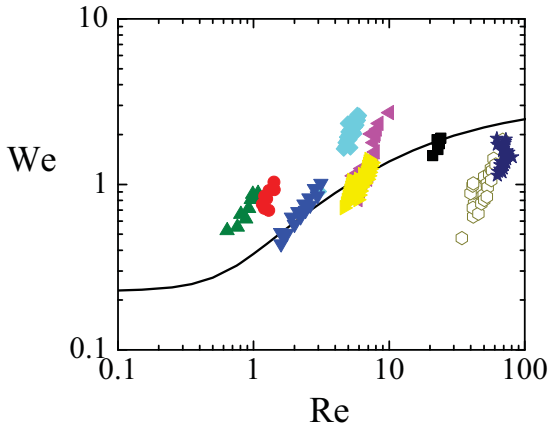

FIG. 7. Reynolds and Weber numbers where monosized dripping was found. The curve corresponds to the convective-to-absolute instability transition [27].

V. SUMMARY

In the classical steady jetting mode of axisymmetric flow focusing, a high-speed gas stream accelerates the liquid injected through a feeding capillary until a thin jet is steadily emitted. Both the liquid jet and the coflowing gas stream cross the discharge orifice located in front of the capillary, whose diameter is much larger than that of the microjet. The Rayleigh capillary instability eventually breaks the jet into droplets with diameters that are commensurate with that of the precursor jet. This technique does not generally provide monodisperse collections of droplets due to fluctuations of the dominant perturbation wavelength, satellite droplets associated with the nonlinearities of the process, and whipping instabilities triggered by the high-speed gas stream for large enough Weber numbers [2]. In order to increase the monodispersity degree of the emitted droplets, the gas speed can be reduced and fixed within a narrow interval where the jetting regime becomes unstable and yields what we have called the monosized dripping mode. In this mode, perfectly monodisperse collections of drops are ejected right behind the discharge orifice, with diameters small enough for varied technological applications. This dripping mode enhances the applicability of the flow focusing technique because it produces droplets less energetic than those formed in the jetting regime, suitable for gentle liquid deposition on solid surfaces or interactions with other droplets. In this paper we derived and experimentally validated the scaling law for the droplet diameter as a function of the governing parameters. We also showed the parameter windows where the monosized dripping mode can be obtained.

The scaling law derived in this work differs from that obtained for the bubbling mode of flow focusing [14]. The fact that the outer phase has a much lower density than the inner one in our system fundamentally changes the problem. In particular, while the radial pressure gradient in the outer phase can be neglected in the liquid-surrounded-by-gas system, this approximation is not valid in the opposite configuration [14].

ACKNOWLEDGMENTS

Partial support from the Ministerio de Economía, Industria y Competitividad and Gobierno de Extremadura (Spain) through Grants No. DPI2013-46485 and No. GR10047, respectively, is gratefully acknowledged.

[1] G. F. Christopher and S. L. Anna, J. Phys. D **40**, R319 (2007).
[2] A. M. Gañán-Calvo, Phys. Rev. Lett. **80**, 285 (1998).
[3] U. Weierstall *et al.*, Nat. Commun. **5**, 3309 (2014).
[4] A. M. Gañán-Calvo, J. M. Montanero, L. Martín-Banderas, and M. Flores-Mosquera, Adv. Drug Delivery Rev. **65**, 1447 (2013).
[5] T. Si, H. Feng, X. Luo, and R. X. Xu, Microfluid. Nanofluid. **18**, 967 (2015).
[6] M. Trebbin, K. Kruger, D. DePonte, S. V. Roth, H. N. Chapman, and S. Forster, Lab Chip **14**, 1733 (2014).
[7] T. P. Forbes and E. Sisco, Analyst **139**, 2982 (2014).
[8] D. P. DePonte, U. Weierstall, K. Schmidt, J. Warner, D. Starodub, J. C. H. Spence, and R. B. Doak, J. Phys. D **41**, 195505 (2008).
[9] H. Duan, F. J. Romay, C. Li, A. Naqwi, W. Deng, and B. Y. H. Liu, Aerosol Sci. Technol. **50**, 17 (2016).
[10] A. Ponce-Torres, J. M. Montanero, E. J. Vega, and A. M. Gañán-Calvo, J. Non-Newtonian Fluid Mech. **229**, 8 (2016).
[11] J. Eggers and E. Villermaux, Rep. Prog. Phys. **71**, 036601 (2008).
[12] S. L. Goren and S. Wronski, J. Fluid Mech. **25**, 185 (1966).
[13] I. Cohen and S. R. Nagel, Phys. Rev. Lett. **88**, 074501 (2002).
[14] A. M. Gañán-Calvo, Phys. Rev. E **69**, 027301 (2004).
[15] S. L. Anna, N. Bontoux, and H. A. Stone, Appl. Phys. Lett. **82**, 364 (2003).
[16] P. Garstecki, H. A. Stone, and G. M. Whitesides, Phys. Rev. Lett. **94**, 164501 (2005).
[17] H. A. Stone, A. Stroock, and A. Ajdari, Annu. Rev. Fluid Mech. **36**, 381 (2004).
[18] B. Ambravaneswaran, S. D. Phillips, and O. A. Basaran, Phys. Rev. Lett. **85**, 5332 (2000).
[19] T. Si, F. Li, X.-Y. Yin, and X.-Z. Yin, J. Fluid Mech. **629**, 1 (2009).
[20] E. J. Vega, J. M. Montanero, M. A. Herrada, and A. M. Gañán-Calvo, Phys. Fluids **22**, 064105 (2010).
[21] P. Huerre and P. A. Monkewitz, Annu. Rev. Fluid Mech. **22**, 473 (1990).
[22] B. Ambravaneswaran, H. J. Subramani, S. D. Phillips, and O. A. Basaran, Phys. Rev. Lett. **93**, 034501 (2004).
[23] A. S. Utada, E. Lorenceau, D. R. Link, P. D. Kaplan, H. A. Stone, and D. A. Weitz, Science **308**, 537 (2005).
[24] A. M. Gañán-Calvo, Appl. Phys. Lett. **86**, 214101 (2005).
[25] M. Strani and F. Sabetta, J. Fluid Mech. **141**, 233 (1984).
[26] A. M. Gañán-Calvo, J. Fluid Mech. **226**, 63 (1991).
[27] S. J. Leib and M. E. Goldstein, Phys. Fluids **29**, 952 (1986).